Computational Mechanics 16 (1995) 328–340 © Springer-Verlag 1995

The *p*-version of finite element method for shell analysis

J. Fish, R. Guttal

Abstract A new quadrature scheme and a family of hierarchical assumed strain elements have been developed to enhance the performance of the displacement-based hierarchical shell elements. Various linear iterative procedures have been examined for their suitability to solve system of equations resulting from hierarchic shell formulations.

1 Introduction

Since early seventies there has been a disagreement between various sections in the finite element community over the computational efficiency of higher order elements. On one hand there was a clear mathematical evidence of the superior theoretical rate of convergence (measured in terms of the problem size) of the *p*-type methods for properly designed meshes as demonstrated by Babuska, Szabo, and Katz (1981) but on the other hand, it was commonly believed, primarily in the engineering community, that the *h*-method is computationally more efficient due to its superior sparsity. The disagreement has peaked in the early nineties. For example, in the First US Congress on Computational Mechanics, Bathe presented numerical results conducted on Floyd pressure vessel showing the superior performance in terms of CPU time of the *h*-method even for problems for which the exact solution is analytic. At the same conference Carnevali reported IBM research division findings on similar problems suggesting exactly an opposite trend.

In practice, computational efficiency of various finite element versions depends not only on sparsity and theoretical rate of convergence, but is a function of several other factors including adaptivity and quality control, conditioning, distortion sensitivity, locking, model preparation and model improvement, utilization of previous computations and coding simplicity. Ironically, there is no general consensus on the relative merits of some of these factors. For example, it has been argued that for *p*-type methods the finite element mesh is simpler, and thus the time required for data preparation is substantially smaller. Unfortunately in automated computational environment the cost of automatic mesh generation of higher order elements is not necessarily lower than that of the *h*-method (Shephard and Dey 1994).

Communicated by S. N. Atluri, 28 April 1995

J. Fish, R. Guttal
Department of Civil Engineering and Scientific Computation Research Center, Rensselaer Polytechnic Institute, Troy, NY 12180. USA

Correspondence to: J. Fish

The *p*-method has been commended for its versatility in the adaptive process due to its ability to exploit previous computations and the elegance of hierarchical error estimation process (Zeinkiewicz and Craig 1986). However, it is often overlooked that the sequence of lower order finite element meshes generated in the adaptive process can be utilized for both solution and quality control processes by utilizing multigrid technology (Brandt 1977).

Contradicting observations were reported regarding the sensitivity to element distortion. Holzer, Rank, and Werner (1990) present experimental results indicating that higher order elements are less sensitive to mesh distortion, while Ramm, Stander and Matzenmiller (1989) in their review article on assumed strain shell formulation report that 4-node bilinear shell elements are less sensitive to mesh distortion than their quadratic counterparts.

In the realm of opposing views, there is a sound theoretical evidence on superior conditioning of matrices arising from orthogonal basis functions (Zeinkiewicz and Craig 1986), and circumvention of locking with higher order elements as shown by Szabo, Babuska, and Chayapaty (1989). Nevertheless, since the overall computational efficiency is strongly linked to the program architecture, it is not obvious what are the contributing factors of these aspects.

The present work focuses on the computational aspects of the *p*-version for shell analysis. The following aspects are studied:

- How to enhance the performance of shell elements up to the polynomial order of 4–5 using assumed strain formulation.
- How to speed up the computation of element matrices by utilizing previous computations and how to exploit hierarchiality of the *p*-method via special quadrature scheme.
- How to exploit the well conditioning of matrices arising from the *p*-method by utilizing the multigrid like technology with various acceleration schemes for thick and thin shells.

2 Element formulation

2.1 Preliminaries

Consider the geometry of a typical quadrilateral shell element defined by the following relation:

$$\mathbf{X} = \tfrac{1}{2}[(1+\xi_3)\,\mathbf{X}^{top}(\xi_1,\xi_2) + (1-\xi_3)\,\mathbf{X}^{bot}(\xi_1,\xi_2)] \qquad (1)$$

2.2.3
Assumed natural strain field

In order to alleviate membrane and shear locking primarily at lower polynomial we define an assumed natural strain interpolants $\bar{\mathbf{B}}_A^{nat} = \{\bar{b}_{Aij}^{nat}\}$ in the following manner: Let (NG_1, NG_2, NG_3) be the number of quadrature points for the displacement based formulation. To enhance the element performance, we introduce a special set of one-dimensional shape functions $[\phi_J(\xi_1), \phi_K(\xi_2), \phi_M(\xi_3)]$ defined with nodes at reduced quadrature points $(\bar{\xi}_{1J}, \bar{\xi}_{2J}, \bar{\xi}_{3K})$ where $J \in [1, NG_1 - 1]$, $K \in [1, NG_2 - 1]$, $M \in [1, NG_3 - 1]$.

The general form of $\{\bar{b}_{Aij}^{nat}\}$ is given by:

$$\bar{b}_{Aii}^{nat} = \sum_{I=1}^{NG_I - 1} b_{Aii}^{nat}(\xi_i = \bar{\xi}_{iI}, \xi_j, \xi_k)\, \phi_I(\xi_i) \quad \text{no sum on i}$$

$$\bar{b}_{Aij}^{nat} = \sum_{I=1}^{NG_I - 1} \sum_{J=1}^{NG_J - 1} b_{Aij}^{nat}(\xi_i = \bar{\xi}_{iI}, \xi_j = \bar{\xi}_{jJ}, \xi_k)\, \phi_I(\xi_i)\, \phi_J(\xi_j)$$

$$i \neq j \quad \text{no sum on i, j} \tag{10}$$

2.2.4
Stiffness matrix calculations

Since the constitutive relations are expressed in material coordinate system, the natural strains are transformed to material coordinate system. From Eqs. (4) and (5), the strain components in material coordinate system are defined as:

$$\Xi_{kl} = \frac{\partial \xi_i}{\partial x_k}\frac{\partial \xi_j}{\partial x_l}\varepsilon_{ij} = \left[\frac{\partial x_k}{\partial \xi_i}\right]^{-1}\left[\frac{\partial x_l}{\partial \xi_j}\right]^{-1}\varepsilon_{ij} \equiv T_{klij}\,\varepsilon_{ij} \tag{11}$$

or

$$\boldsymbol{\Xi} = \mathbf{T}\,\boldsymbol{\varepsilon} \tag{12}$$

and the element stiffness matrix can be cast into the classical form:

$$\mathbf{K}^e = \int_\Omega \bar{\mathbf{B}}^{nat^T}\mathbf{D}^e\bar{\mathbf{B}}^{nat}\,d\Omega$$

where $\bar{\mathbf{B}}^{nat}$ is defined by Eq. (10) and

$$\mathbf{D}^e = \mathbf{T}^T\mathbf{D}^{\bar{\Xi}}\mathbf{T} \tag{13}$$

$\mathbf{D}^{\bar{\Xi}}$ is the constitutive matrix defined in the Material coordinate system.

2.3
H3RANS–Hierarchical (3 – *D*) reduced transverse stiffness, Assumed Natural Strain element

For the purpose of examining the causes of somewhat stiffer behavior of H3-type elements compared to their degenerated counterparts (Stanley, Levitt, Stehlin, and Hurlbut 1992), we consider a beam problem. For elastic isotropic beam the strain energy is given by,

$$U = \frac{1}{2}\int_L (D_B\kappa^2 + D_M\varepsilon^2 + D_S\gamma^2)\,dx \tag{14}$$

where L is the element length; ε, κ, and γ are the membrane strain, curvature and transverse shear strain respectively; D_B, D_M, and D_S are the bending, membrane and shear stiffness constants given by,

$$D_B = \frac{Et^3}{12} \quad D_M = Et \quad D_S = k_s Gt \tag{15}$$

where t is the thickness of the beam of a unit width; E the Youngs modulus; G the shear modulus and k_s the shear correction factor.

In the classical beam formulation the normal strains μ are *a posteriori* calibrated to maintain zero normal stress (plane stress assumption), and thus have no contribution to the strain energy in Eq. (14). It can be seen that as $t \to 0$ the bending energy becomes negligible in comparison to shear and membrane energy giving rise to shear and membrane locking, if the element cannot represent deformed state in which shear and membrane strains vanish through out the element (Belytschko, Stolarski, Liu, Carpenter, and Ong 1985).

In H3-type beam elements normal strains are computed directly from kinematics. These values are not arbitrary and cannot be calibrated to maintain plane stress condition. Thus if two dimensional state of stress is considered, the resulting strain energy takes the following form:

$$U = \frac{1}{2}\int_L (\bar{D}_B\kappa^2 + \bar{D}_M\varepsilon^2 + \varepsilon D_C\mu + D_S\gamma^2 + D_\mu\mu^2)\,dx \tag{16}$$

It can be seen that in H3-type flexural elements spurious coupling between membrane and normal deformation exists giving rise to a parasitic transverse normal strain energy, which is of the same order of magnitude as that of the membrane strain energy if the strains are of equal order. This phenomenon is referred here as the transverse normal locking of H3-type flexural elements.

To ameliorate the locking caused by the transverse normal strains we propose to calibrate the constitutive behavior of H3-type elements to match the strain energy corresponding to H2-type elements without introducing zero energy modes. This is accomplished by modifying coefficients in constitutive tensor in the following way:

$$\bar{D}_M = D_M \quad \bar{D}_B = D_B \quad D_C = 0 \quad D_\mu = \chi D_M \tag{17}$$

where χ is a stabilization parameter aimed at stabilizing the zero transverse normal energy modes of H3-type flexural elements.

2.4
H2ANS–Hierarchic (2 – *D*) Degenerated Assumed Natural Strain element with rotational degrees-of-freedom

In this section we attempt to formulate a degenerated assumed strain shell element, which employs blending functions or Lagrangian basis for geometry mapping and Legendre polynomials for solution interpolation.

As a starting point, the displacement field is expressed in terms of mid-point translations $u_i^t(\xi_1, \xi_2)$ and mid-point rotations $\theta_\alpha(\xi_1, \xi_2)$ which are defined with respect to the fiber coordinate system:

$$\begin{Bmatrix} u_1 \\ u_2 \\ u_3 \end{Bmatrix}_{(\xi_1,\xi_2,\xi_3)} = \begin{Bmatrix} u_1^t \\ u_2^t \\ u_3^t \end{Bmatrix}_{(\xi_1,\xi_2)} + \frac{\xi_3}{2}[-t\mathbf{e}_2^f, t\mathbf{e}_1^f]_{(\xi_1,\xi_2)}\begin{Bmatrix}\theta_1 \\ \theta_2\end{Bmatrix} \tag{18}$$

Proof. Substituting (20) and (21) into left hand side of (22) yields:

$$\int_\Omega (gh)\,d\Omega = \sum_{i=0}^{n_1}\sum_{j=0}^{n_2}\sum_{k=0}^{n_3}\sum_{s=0}^{m_1}\sum_{t=0}^{m_2}\sum_{r=0}^{m_3} a_{ijk}\,b_{rst}$$

$$\cdot \underbrace{\int_{-1}^{+1} \hat{P}_i(\xi_1)\,\hat{P}_r(\xi_1)\,d\xi_1}_{\delta_{ir}} \underbrace{\int_{-1}^{+1} \hat{P}_j(\xi_2)\,\hat{P}_s(\xi_2)\,d\xi_2}_{\delta_{js}}$$

$$\cdot \underbrace{\int_{-1}^{+1} \hat{P}_k(\xi_3)\,\hat{P}_t(\xi_3)\,d\xi_3}_{\delta_{kt}}$$

$$= \sum_{i=0}^{l_1}\sum_{j=0}^{l_2}\sum_{k=0}^{l_3} a_{ijk}\,b_{ijk} = \sum_{I=1}^{L} a_I\,b_I \qquad (23)$$

Likewise, the right hand side of (22) gives:

$$\sum_{I=1}^{L}\int_\Omega g\phi_I\,d\Omega \int_\Omega h\phi_I\,d\Omega$$

$$= \sum_{i=0}^{l_1}\sum_{j=0}^{l_2}\sum_{k=0}^{l_3}\sum_{s=0}^{n_1}\sum_{t=0}^{n_2}\sum_{r=0}^{n_3}\left(a_{str}\int_{-1}^{1} \hat{P}_i(\xi_1)\,\hat{P}_s(\xi_1)\,d\xi_1 \right.$$

$$\left. \cdot \int_{-1}^{1} \hat{P}_j(\xi_2)\,\hat{P}_t(\xi_2)\,d\xi_2 \int_{-1}^{1} \hat{P}_k(\xi_3)\,\hat{P}_r(\xi_3)\,d\xi_3 \right)$$

$$\cdot \sum_{p=0}^{m_1}\sum_{q=0}^{m_2}\sum_{v=0}^{m_3}\left(b_{pqv}\int_{-1}^{1} \hat{P}_i(\xi_1)\,\hat{P}_p(\xi_1)\,d\xi_1 \int_{-1}^{1} \hat{P}_j(\xi_2)\,\hat{P}_q(\xi_2)\,d\xi_2 \right.$$

$$\left. \cdot \int_{-1}^{1} \hat{P}_k(\xi_3)\,\hat{P}_v(\xi_3)\,d\xi_3 \right) = \sum_{i=0}^{l_1}\sum_{j=0}^{l_2}\sum_{k=0}^{l_3} a_{ijk}\,b_{ijk} = \sum_{I=1}^{L} a_I\,b_I \qquad (24)$$

The dot product of integral decomposition was originally proposed by Hinnant (1993). The quadrature based on dot product integral decomposition is optimal in terms of number of integrand evaluations for hierarchical systems. To clarify this point we consider a one-dimensional case. Let $\mathbf{g} = \{g_i\}$ and $\mathbf{h} = \{h_j\}$ be vectors whose terms represent the hierarchical sequence with increasing polynomial order, where subscripts on g and h denote the polynomial orders and $i, j \in [0, p]$. In evaluating integrals of the form $G_{ik} = \int g_i \hat{P}_k(\xi)\,d\xi$ and $H_{jl} = \int h_j \hat{P}_l(\xi)\,d\xi$, where $k \in [0, i]$ and $l \in [0, j]$, the number of function evaluations for (g_i, h_j) is $(i+1)$ and $(j+1)$, respectively. Thus the total number of function evaluations for computing all the integrals of the form G_{ik} and H_{jl} is $(p+1)(p+2)$ as opposed to $2(p+1)^2$ for uniform quadrature. It can be shown that this estimate grows exponentially with the increase in the number of space dimensions.

The major drawback of Dot product integral decomposition is the lack of symmetry, which leads to:

1. Non-symmetric stiffness matrix if $\mathbf{g}$ and $\mathbf{h}$ are of different polynomial orders (such a situation may arise in the case of material or geometric nonlinearity).
2. Redundancy in evaluating each of the two integrals G_{ik} and H_{jl}, which, except for the term involving constitutive tensor, should be identical.

3.3
Symmetric dot product integral decomposition

In this section we present a variant of Dot product integral decomposition which preserves the symmetry of the stiffness matrix. Consider a typical stiffness term given by

$$k_{AB} = \int_\Omega \underbrace{\mathbf{B}_A^T \mathbf{D}\,\mathbf{B}_B\,J}_{\mathbf{g}_A \mathbf{h}_B}\,d\Omega \qquad (25)$$

In an attempt to obtain a symmetric dot product integral decomposition, we decompose the integrand $(\mathbf{g}_A\,\mathbf{h}_B)$ as follows:

$$\mathbf{h}_A^T = \mathbf{g}_A = \mathbf{B}_A^T \mathbf{L}\,J^{1/2} \qquad (26)$$

where $\mathbf{L}$ is a lower triangular Cholesky factor of the constitutive matrix $\mathbf{D}$. The resulting stiffness matrix is given by

$$k_{AB} = \sum_{I=1}^{L}\int_\Omega (\mathbf{L}^T\mathbf{B}_A)^T \phi_I J^{1/2}\,d\Omega \int_\Omega \mathbf{L}^T\mathbf{B}_B\,\phi_I J^{1/2}\,d\Omega \qquad (27)$$

Each of the integrals is integrated using Gauss quadrature. The number of quadrature points as well as the maximum polynomial order of the interpolating Legendre polynomials in each direction depends on how well the integrand $\mathbf{L}^T\,\mathbf{B}_A\,J^{1/2}$ is approximable by polynomials and what is their polynomial order. We will refer to this integration scheme as Symmetric Dot Product (SDP) Gauss quadrature.

In case when the constitutive tensor $\mathbf{D}$ is not positive definite an alternative integrand decomposition is employed. Let

$$\mathbf{g}_A = \mathbf{B}_A^T J^{1/2} \quad \mathbf{h}_B = \mathbf{D}\,J^{1/2}\,\mathbf{B}_B \qquad (28)$$

yielding

$$k_{AB} = \sum_{I=1}^{L}\int_\Omega \mathbf{B}_A^T J^{1/2}\,\phi_I\,d\Omega \int_\Omega \overbrace{\mathbf{D}\,\phi_I}^{\mathbf{g}_I}\,\underbrace{\mathbf{B}_B J^{1/2}}_{\mathbf{h}_B}\,d\Omega \qquad (29)$$

and further dot product integral decomposition of the second term in (29) yields the following symmetric form:

$$k_{AB} = \sum_{I=1}^{L}\sum_{J=1}^{L}\int_\Omega (\mathbf{B}_A^T J^{1/2})\,\phi_I\,d\Omega \cdot \int_\Omega \underbrace{(\mathbf{D})\,\phi_I\,\phi_J\,d\Omega}_{\bar{\mathbf{D}}_{IJ}} \cdot \int_\Omega (\mathbf{B}_B^T J^{1/2})\,\phi_J\,d\Omega \qquad (30)$$

Note that if the constitutive tensor is constant, $\bar{\mathbf{D}}_{IJ} = \int_\Omega (\mathbf{D})\,\phi_I\,\phi_J\,d\Omega = \mathbf{D}\,\delta_{IJ}$ reducing Eq. (30) to

$$k_{AB} = \sum_{I=1}^{L}\int_\Omega (\mathbf{B}_A^T J^{1/2})\,\phi_I\,d\Omega \cdot \mathbf{D} \cdot \int_\Omega (\mathbf{B}_B^T J^{1/2})\,\phi_I\,d\Omega \qquad (31)$$

In can be easily shown that if $\mathbf{D} \neq$ constant, stiffness matrix evaluations by means of Eq. (30) is more computationally intensive because of the double summation involved. Nevertheless, the triple integral decomposition (30) might be useful in the following two scenarios:

- Thick laminated composite shells with multiple layers and variable jacobian through the thickness.
- Small deformation nonlinear material analysis, where the first term in (30) can be computed only once and then reused in the nonlinear incremental iterative process.

$\mathbf{Q}_m^{m-1}$ and $\mathbf{Q}_{m-1}^m$ be the restriction and prolongation operators, which transfer the data from level (m) to level $(m-1)$ and vice versa. For the p-method it has a very simple form:

$$\mathbf{Q}_m^{m-1} = [\mathbf{I} \quad \mathbf{0}] = \mathbf{Q}_{m-1}^{m\,T} \tag{39}$$

where $\mathbf{I}$ is the order n_{m-1} identity matrix, and $\mathbf{0}$ is order $(n_m - n_{m-1})$ zero matrix. Note that the restriction of the stiffness matrix is given by:

$$\hat{\mathbf{K}}^{m-1} = \mathbf{Q}_m^{m-1}\mathbf{K}^m\mathbf{Q}_{m-1}^m \neq \mathbf{K}^{m-1} \tag{40}$$

A single V-cycle has a compact recursive definition given by:

$$\mathbf{z}^m := MG^m(\mathbf{r}^m, \mathbf{K}^m). \tag{41}$$

where $\mathbf{r}^m$ is the residual vector. The V-cycle multigrid algorithm is summarized below:

1. Loop $i = 0, 1, 2 \ldots$ until convergence
   if $i = 0 \leftarrow \mathbf{d}^m = 0$
2. perform γ_1 pre-smoothing operations

   $${}_{\gamma_1}{}^i\mathbf{d}^m := \text{smooth}({}_{\gamma_{1,0}}{}^i\mathbf{d}^m, \mathbf{K}^m, \mathbf{f}^m)$$

   where the left superscript and subscript denote the cycle number and smoothing count respectively.
3. Restrict residual from level m to $m-1$

   $$\mathbf{r}^{m-1} = \mathbf{Q}_m^{m-1}(\mathbf{f}^m - \mathbf{K}^m\,{}_{\gamma_1}{}^i\mathbf{d}^m)$$

4. Coarse grid correction
   If $(m-1)$ = lowest level, solve directly $\mathbf{z}^{m-1}$
   $= (\mathbf{K}^{m-1})^{-1}\mathbf{r}^{m-1}$,
   Else $\mathbf{z}^{m-1} := MG^{m-1}(\mathbf{r}^{m-1}, \mathbf{K}^{m-1})$
5. Prolongate from level $m-1$ to m

   $${}_{\gamma_1+1}{}^i\mathbf{d}^m = {}_{\gamma_1}{}^i\mathbf{d}^m + {}^i\omega\mathbf{Q}_{m-1}^m\mathbf{z}^{m-1}$$

   where ${}^i\omega$ is a coarse grid relaxation parameter, which minimizes energy functional along the prescribed direction $\mathbf{v}^m = \mathbf{Q}_{m-1}^m\mathbf{z}^{m-1}$. Note that for two grid methods ${}^i\omega = 1$ if $\hat{\mathbf{K}}^{m-1} = \mathbf{K}^{m-1}$. Otherwise

   $${}^i\omega = \frac{\mathbf{v}^{m\,T}(\mathbf{f}^m - \mathbf{K}^m\,{}_{\gamma_1+1}{}^i\mathbf{d}^m)}{\mathbf{v}^{m\,T}\mathbf{K}^m\mathbf{v}^m} \tag{42}$$

6. Perform γ_2 post-smoothing operations

   $${}^{i+1}{}_0\mathbf{d}^m := \text{smooth}(\gamma_2, {}_{\gamma_1+1}{}^i\mathbf{d}^m, \mathbf{K}^m, \mathbf{f}^m)$$

A variant of the standard V-cycle multigrid method (Brandt 1977) has been proposed by Bank, Dupont and Yserentant (1988). The method termed as hierarchical basis multigrid technique (HBM), is similar to the standard multigrid V-cycle, except that a smaller than the normal subset of unknowns is updated during the smoothing phase at a given level. HBM takes advantage of the fact that smoothing mainly affects highest oscillatory modes of error, and thus relaxation sweeps are performed on the block by block level keeping the rest of the degrees of freedom fixed. It has been shown by Bank, Dupont and Yserentant (1988) that the rate of convergence of HBM method has a logarithmic dependence on the problem size as opposed to multigrid method which has an optimal rate of convergence independent of the mesh size and spectral order. The key question is whether the benefit from reducing the cost of smoothing process over weighs the suboptimal performance of HBM in comparison with the standard multigrid method for thin and thick shells.

4.2
Two parameter acceleration of multigrid method

For ill-conditioned problems, such as thin shells, it is desirable to accelerate the rate of convergence of the multigrid like methods. In this section we present a two parameter acceleration scheme that requires a small fraction of computational effort, but at the same time is efficient in expediting the convergence of the multigrid like methods (MG and HBM).

Let ${}^i\mathbf{r}^m$ be the residual vector at the end of i^{th} m-level multigrid cycle. The incremental multigrid solution for the next cycle ${}^i\mathbf{z}^m = MG^m({}^i\mathbf{r}^m, \mathbf{K}^m)$ is used as a predictor in the two parameter acceleration scheme. The solution in the correction phase is then updated as follows:

$${}^{i+1}\mathbf{v} = {}^i\alpha\,{}^i\mathbf{z}^m + {}^i\beta\,{}^i\mathbf{v} \tag{43}$$

$${}^{i+1}\mathbf{d}^m = {}^i\mathbf{d}^m + {}^{i+1}\mathbf{v} \tag{44}$$

where parameters $({}^i\alpha, {}^i\beta)$ are obtained by minimizing the potential energy functional:

$$\frac{1}{2}({}^i\mathbf{d}^m + {}^i\alpha{}^i\mathbf{z}^m + {}^i\beta{}^i\mathbf{v})^T\mathbf{K}^m({}^i\mathbf{d}^m + {}^i\alpha\,{}^i\mathbf{z}^m + {}^i\beta{}^i\mathbf{v})$$

$$-({}^i\mathbf{d}^m + {}^i\alpha{}^i\mathbf{z}^m + {}^i\beta{}^i\mathbf{v})^T\mathbf{f}^m \rightarrow \min_{{}^i\alpha\,{}^i\beta} \tag{45}$$

The resulting algorithm is summarized below:

Step 1

$${}^0\mathbf{d}^m = 0, \quad {}^0\mathbf{r}^m = \mathbf{f}^m$$

$${}^0\mathbf{z}^m := MG^m({}^0\mathbf{r}^m, \mathbf{K}^m)$$

$${}^0\mathbf{v} = {}^0\mathbf{y} = 0$$

$${}^0\mathbf{x} = \mathbf{K}^m\,{}^0\mathbf{z}^m$$

$${}^0\beta = 0; \quad {}^0\alpha = \frac{(\mathbf{f}^m, {}^0\mathbf{z}^m)}{({}^0\mathbf{x}^m, {}^0\mathbf{z}^m)} \tag{46}$$

Step 2 Do $i = 0, 1, 2, \ldots$ until convergence

$$\begin{Bmatrix} {}^i\alpha \\ {}^i\beta \end{Bmatrix} = \begin{bmatrix} ({}^i\mathbf{x}, {}^i\mathbf{z}^m) & ({}^i\mathbf{x}, {}^i\mathbf{v}) \\ ({}^i\mathbf{x}, {}^i\mathbf{v}) & ({}^i\mathbf{y}, {}^i\mathbf{v}) \end{bmatrix}^{-1} \begin{Bmatrix} ({}^i\mathbf{r}^m, {}^i\mathbf{z}^m) \\ ({}^i\mathbf{r}^m, {}^i\mathbf{v}) \end{Bmatrix} \quad i > 0 \tag{47}$$

$${}^{i+1}\mathbf{v} = {}^i\alpha\,{}^i\mathbf{z}^m + {}^i\beta\,{}^i\mathbf{v}$$

$${}^{i+1}\mathbf{d}^m = {}^i\mathbf{d}^m + {}^{i+1}\mathbf{v}$$

$${}^{i+1}\mathbf{y} = {}^i\alpha\,{}^i\mathbf{x} + {}^i\beta\,{}^i\mathbf{y}$$

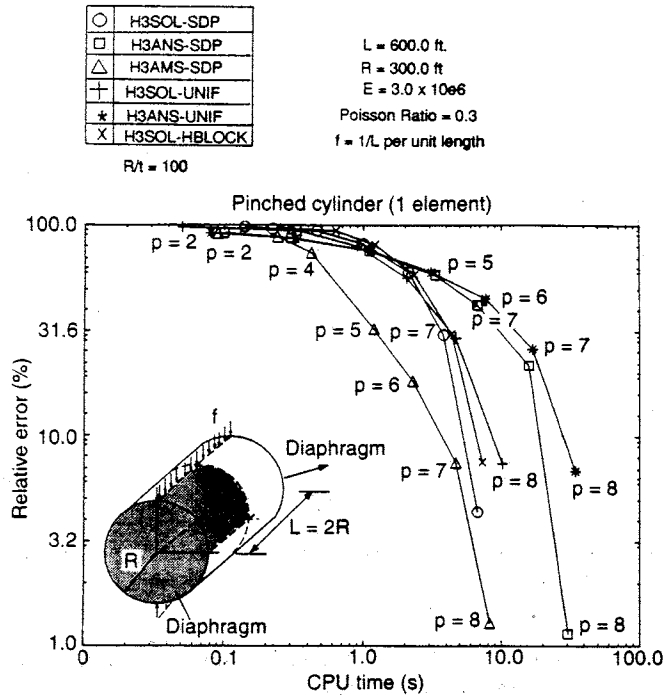

Fig. 3. Comparison of quadrature schemes for **H3R**-type ($q = 1$) elements for pinched cylinder problem

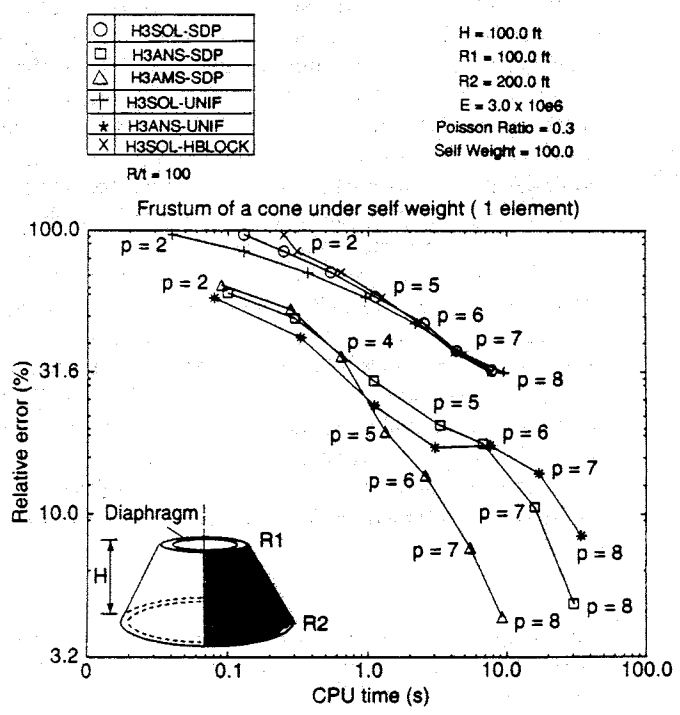

Fig. 4. Comparison of quadrature schemes for **H3R**-type ($q = 1$) elements for frustum of a cone

Each figure contains six plots:

- (○) HSOL-SDP corresponding to Symmetric Dot Product Gauss quadrature for displacement based element.
- (□) HANS-SDP corresponding to Symmetric Dot Product Gauss quadrature for assumed natural strain element.
- (△) HAMS-SDP corresponding to Symmetric Dot Product Gauss quadrature for assumed material strain element.
- (+) HSOL-UNIF corresponding to Uniform Gauss quadrature scheme for displacement based element.
- (*) HANS-UNIF corresponding to Uniform Gauss quadrature scheme for assumed natural strain element.
- (×) HSOL-HBLOCK corresponding to Hierarchic Block Gauss quadrature scheme for displacement based element.

To preserve hierarchical structure of the stiffness matrix the displacement based shell element has been integrated to accommodate for highly varying metric tensor components $\partial x_i/\partial \xi_j$. For numerical examples considered, the number of integration points for Block Gauss quadrature was selected as $p^{max} + 3$ in inplane direction and $q^{max} + 1$ in transverse direction, where p^{max} and q^{max} are the maximum polynomial orders of the corresponding block in inplane and transverse directions, respectively.

Similarly, for SDP-Gauss quadrature applied to displacement based elements, the order of interpolating Legendre polynomials $\hat{P}_i(\xi_i)$ is selected as $(p_i + l)$ $i \in [1, 2]$ in inplane directions and $(q + m)$ in transverse direction. The corresponding number of integration points are $(p_i + l + 1)$ and $(q + m + 1)$ in inplane and transverse directions, respectively, where (p_1, p_2) are the polynomial orders of the integrand in inplane directions (ξ_1, ξ_2) and q is the polynomial order in transverse direction (ξ_3). Selection of integers l and m is dictated by the variation of the metric tensor $\partial x_i/\partial \xi_j$ in inplane and transverse directions respectively. For example, in case of constant inplane jacobian (the pinched cylinder) we used $l = 1$, $m = 0$ and $l = 2$, $m = 1$ for the case of variable inplane jacobian (frustum of the cone).

In case of HAMS elements the order of interpolating Legendre polynomials is selected such that their polynomial order does not exceed the maximum polynomial order of the basis functions to ensure effectivity of selective polynomial order reduction. On the other hand for lower order blocks the polynomial order for Legendre polynomials is selected the same as for displacement based elements to partially preserve hierarchiality. Thus the order of Legendre polynomials for HAMS element is defined using the following rule:

- For a given integrand with polynomial orders (p_i, q)

  The inplane polynomial order of $\hat{P}_i$

$$= \begin{cases} p_i + l & \text{if } p_i + l < p^{\max} \\ p^{\max} & \text{otherwise} \end{cases} \tag{48}$$

  The order of Legendre polynomials in transverse direction is selected as $q + m$.
- The number of inplane integration points is selected as $p^{max} + 1$, and $q^{max} + 1$ in transverse direction.

It is evident from Figs. (1-4) that among the displacement (HSOL) based elements, SDP and HBLOCK quadrature schemes are computationally more efficient than the uniform (UNIF) quadrature. The difference between HSOL-SDP and HSOL-HBLOCK is not significant and it can be deduced that for displacement based elements SDP and HBLOCK have a comparable performance. It is apparent from the Figs. (1-4) that HAMS-SDP has higher computational efficiency than

Table 2. Effect of radius to thickness (R/t) ratio on iterative methods. Three cyclinder assembly modeled with 36 (H2AMS) elements

Solver	(R min/t = 100)	(R min/t = 1000)
MG-GS-ACC(4, 6, 8)	300/25	13728/1144
HBM-GS-ACC(4, 6, 8)	271/37	47879/6537
MG-ICC-ACC(4, 6, 8)	**235/12**	1191/97
HBM-ICC-ACC(4, 6, 8)	250/33	1476/294
PCG-ICC	330/144	1115/660
Direct	536/1	**536/1**

Table 4. Influence of smoothing procedures of Multigrid-like solvers. Pinched cylinder modeled with 16 (H2AMS) elements, Multigrid-like solvers with (4, 6, 8) levels

Solver	GS-1	JPCG-1	ICC
MG-ACC(R/t = 10)	**37/12**	57/17	61/6
HBM-ACC(R/t = 10)	**23/10**	29/11	32/12
MG-ACC(R/t = 100)	115/43	295/97	**110/21**
HBM-ACC(R/t = 100)	117/72	157/76	**110/58**
MG-ACC(R/t = 300)	797/315	1359/445	**245/59**
HBM-ACC(R/t = 300)	632/412	447/221	**310/182**

performance of the iterative procedures deteriorates, due to increase in the condition number. Assuming that deterioration in conditioning does not affect the accuracy of direct solution due to round off errors, the direct solver has outperformed the iterative procedures for very thin shells ($R/t = 1000$).

In Table 4 the influence of various popular smoothing procedures (GS – Gauss Seidel; JPCG – Jacobi pre-conditioned conjugate gradient and ICC – Incomplete Cholesky) on the performance multigrid-like solvers (MG-ACC and HBM-ACC) is examined. One smoothing iteration of each procedure is incorporated. The experiments are conducted on the pinched cylinder problem modeled with 16 elements with $R/t = 10$; $R/t = 100$ and $R/t = 300$. For either of the multigrid procedures one Incomplete Cholesky (ICC) smoothing has been found to be optimal in terms of CPU time for both thin ($R/t = 100$) and very thin ($R/t = 300$) shells. For relatively thick shells ($R/t = 10$) the weaker Gauss Seidel smoothing is found to be optimal in terms of CPU time.

In Table 5 we study the performance of multigrid solver (MG-GS-ACC) for the case where the coarse mesh represents the state of plane stress ($p = 8$, $q = 1$) while the fine mesh represents 3-D model with ($p = 8$, $q = 3$). The coarse grid relaxation parameter defined in Eq. (42) is used for efficient coarse grid correction. Alternatively, one can recompute and factorize the stiffness matrix corresponding to $q = 1$ with a 3-D constitutive model and then incorporate it for coarse grid correction. For a relatively small problem considered (12 elements, 2208 dofs for $q = 1$) no significant difference in terms of CPU time has been found between the two methods. Numerical experiments indicate that HBM-ACC is not particularly well suited for transitioning between different mathematical models.

Table 5. Study of Multigrid-like solvers for transitioning from plane stress to 3-D models. pinched cylinder modeled with 12 (H3) elements, Multigrid-like solver MG-GS-ACC with 2 Gauss Seidel smoothing

Element	NDOFS	Direct	2D – 3D	Recomputed
H3RAMS (q = 3)	4416	1203	904/55	**877/41**
H3SOL (q = 3)	4416	1203	**789/48**	906/46

Figures 7 and 8 depict the rate of convergence of various elements for the pinched cylinder and the 3 cylinder assembly problems respectively. Percentage relative error in the energy norm is plotted versus the total CPU time required to solve the problem. SDP quadrature scheme for integration of element stiffness matrices and the best solution procedure for a given polynomial order are adopted for all elements. It is evident that H2AMS and H3RAMS have the best performance in degenerated and 3-D categories, respectively.

6 Summary and conclusions

Research efforts have been made to optimize the computational efficiency of the p-method for shell analysis. A new quadrature scheme and a family of hierarachical assumed strain based shell elements have been introduced. Various linear iterative procedures have been examined for their suitability to solve linear system of equations resulting from hierarchic shell formulation.

In Figs. 9 and 10 we compare h and p versions of finite element analysis for the two shell problems, a pinched cylinder

Table 3. Effect of radius to thickness (R/t) ratio on iterative methods. Pinched cylinder modeled with 16 (H2AMS) elements

Solver: R/t =	10	20	30	100	300	1000
MG-GS-ACC(4, 6, 8)	37/12	48/16	57/20	115/43	797/315	5004/1969
HBM-GS-ACC(4, 6, 8)	**23/10**	**33/16**	**37/19**	117/72	632/412	5098/3357
MG-ICC-ACC(4, 6, 8)	61/6	65/7	68/8	**110/21**	245/59	610/171
HBM-ICC-ACC(4, 6, 8)	32/12	38/15	45/20	**110/58**	310/182	862/517
PCG(4, 6, 8)	148/24	164/36	187/52	425/232	827/458	1953/1329
PCG-ICC	50/22	60/34	65/42	130/135	258/324	623/860
Direct	242/1	242/1	242/1	242/1	242/1	**242/1**
MG-ICC-ACC(6, 8)	155/5	158/6	158/6	177/12	**235/33**	416/98
HBM-ICC-ACC(6,8)	130/7	134/9	139/12	171/30	271/87	541/238
PCG(6, 8)	171/12	184/19	200/30	370/133	532/255	1112/481

References

Babuska, I.; Szabo, B. A.; Katz, I. N. 1981: The *p*-version of the finite element method. SIAM J. Numer. Anal. 18: 512–545

Baker, V. A.; Axelsson, O. 1984: Finite Element Solution of Boundary Value Problem. Academic Press Inc. NY

Bank, R. E.; Dupont, T. F.; Yserentant, H. 1988: The hierarchical basis multigrid method. Numer. Math. 52: 427–458

Belytschko, T.; Stolarski, H.; Liu, W. K.; Carpenter, N.; Ong, J. S.-J. 1985: Stress projection for membrane and shear locking in shell finite elements. Comp. Meth. in Appl. Mech. and Engg. 51: 221–258

Brandt, A. 1977: Multi-level adaptive solutions to boundary-value problems. Mathematics of Computation, 31: 333–390

Carnevali, P.; Morris, R. B.; Tsuji, Y.; Taylor, G. 1992: New Basis Functions and Computational Procedures for *p*-type Finite Element Analysis. RJ 8710 (78272) Engineering Technology. April 3, 1992

Hinnant, H. E. 1993: A Fast method of numerical quadrature for *p*-version finite element matrices. A.I.A.A. 1386.

Holzer, S.; Rank, E.; Werner, H. 1990: An implementation of the *hp*-version of the finite element method for Reissner-Mindlin plate problems. Int. J. Numer. Methods Eng. 30: 459–471

Hughes, T. J. R. 1987: The Finite Element Method. Prentice-Hall.

Park, K. C.; Stanley, G. M. 1986: A curved C^0 Shell element based on Assumed Natural Coordinate Strains. J. of Appl. Mech. 108: 278–290

Ramm, E.; Stander, N.; Matzenmiller, A. 1989: An assessment of Assumed strain methods in finite rotation shell analysis. Eng. Comput. 6

Shephard, M. S.; Dey, S. 1994: Geometric mapping of finite elements on shell geometry. SCOREC report 15

Stanley, G. M.; Levitt, I.; Stehlin, B.; Hurlbut, B. 1992: Adaptive Analysis of Composite Shell Structures via Thickness-tailored 3D Finite Elements. Winter Annual Meeting Anaheim, CA, November 11–13, 1992

Surana, K. S.; Sorem, R. M. 1991: *p*-version hierarchical three dimensional curved shell element for elastostatics. Int. J. Numer. Methods Eng. 31: 649–676

Szabo, B. A.; Sahrmann, G. J. 1988: Hierarchic plate and Shell models based on *p*-extensions. Int. J. Numer. Methods Eng. 26: 1855–1881

Szabo, B. A.; Babuska, I.; Chayapaty, B. K. 1989: Stress computations for nearly incompressible materials by the *p*-version of the Finite Element method. Int. J. Numer. Methods Eng. 28: 2175–2190

Zeinkiewicz, O. C.; Craig, A. 1986: Adaptive Refinement, Error Estimates, Multigrid Solution, and Hierarchic Finite Element Method Concepts. In Babuska, I. Zeinkiewicz, O. C. Gago, J.; Oliveira, E. R. de A. eds. Accuracy Estimates and Adaptive Refinements in Finite Element Computations